Solid-State Coordination Chemistry: Influences of {M(terpyridyl)} (M = Fe(III), Cu(II), Ni(II)} Subunits on Molybdenum Oxide Structures

Pamela J. Hagrman and Jon Zubieta*

Department of Chemistry, Syracuse University, Syracuse, New York 13244

Received February 28, 2000

The hydrothermal reactions of $Na_2MoO_4 \cdot 2H_2O$ and 2,2′:6′,2″-terpyridine with appropriate salts of Fe(II), Cu(II), and Zn(II) yield a variety of mixed metal oxide phases. The Cu(II) system affords the molecular cluster [Cu(terpy)MoO_4]·$3H_2O$ (MOXI-40·$3H_2O$), as well as a one-dimensional material [Cu(terpy)Mo_2O_7](**MOXI-41**) which is constructed from $\{Mo_4O_{14}\}^{4-}$ clusters linked through $\{Cu(terpy)\}^{2+}$ units. In constrast, the Zn(II) phase of stoichiometry identical to that of **MOXI-41**, [Zn(terpy)Mo_2O_7](**MOXI-42**), exhibits a one-dimensional structure characterized by a $\{Mo_2O_7\}_n^{2n-}$ chain decorated with peripheral $\{Zn(terpy)\}^{2+}$ subunits. The iron species [{Fe(terpy)}$_2$$Mo_4O_{12}$](**MOXI-43**) is also one-dimensional but exhibits $[\{Fe(terpy)\}_2\{MoO_4\}_2]^{2+}$ rings linked through $\{MoO_4\}^{2-}$ tetrahedra. A persistent structural motif which appears in **MOXI-40**, **MOXI-41,** and **MOXI-43** is the $[\{M(terpy)\}_2\{MoO_4\}_2]^n$ cluster with a cyclic $\{M_2Mo_2O_4\}$ core. In general, the secondary metal sites M(II, III) are effective bridging groups between molybdate subunits of varying degrees of aggregation. Furthermore, the ligands passivate the bimetallic oxide from spatial extension in two or three dimensions and provide a routine entree into low-dimensional structural types of the molybdenum oxide family of materials.

Introduction

Metal oxides are ubiquitous compounds whose vast scope of stoichiometries and structure types result in a range of useful physical properties and applications to materials as diverse as magnetic oxides, sensors, phosphors, ceramics, catalysts, ion exchanges, and molecular sieves and even biomaterials.[1−24] The continued evolution of the functional complexity of inorganic oxides requires synthetic strategies for the modification of oxide structure and the appropriate juxtaposition of reactive centers. A powerful tool for the design of novel oxide materials exploits the incorporation of organic molecules to alter the inorganic microstructure or to transmit structural information inherent in the coordination preferences of the metal centers. Examples of the structure-directing role of organic constituents on oxide microstructures include zeolites,[25] biomineralized materials,[26] mesoporous compounds of the MCM-41 class,[27] and transition metal phosphates.[28,29]

A related approach which we have developed for the synthesis of organically modified molybdenum and vanadium oxides may be described as solid-state coordination chemistry.[30] Several types of oxide materials are evolving from this variant of small molecule synthesis: (a) solids constructed from molecular building blocks, represented by polyoxoanion clusters linked through secondary metal−ligand moieties acting as inorganic bridging groups;[31−35] (b) inorganic oxides encapsulated within

(1) Reynolds, T. G.; Buchanan, R. C. In *Ceramic Materials for Electronics*, 2nd ed.; Buchanan, R. C., Ed.; Dekker: New York, 1991; p 207.
(2) Büchner, W.; Schliebs, R.; Winter, G.; Büchel, K. H. *Industrial Inorganic Chemistry*; VCH: New York, 1989.
(3) McCarroll, W. H. In *Encyclopedia of Inorganic Chemistry*; King, R. B., Ed.; John Wiley and Sons: New York, 1994; Vol. 6, p 2903.
(4) Haertling, G. H. In *Ceramic Materials for Electronics*, 2nd ed.; Buchanan, R. C., Ed.; Dekker: New York, 1991; p 129.
(5) Leverenz, H. W. *Luminescence of Solids*; Wiley: New York, 1980.
(6) Einzinger, R. *Annu. Rev. Mater. Sci.* **1987**, *17*, 299.
(7) Tarascon, J. M.; Barboux, P.; Miceli, P. F.; Greene, L. H.; Hull, G. W.; Eibschutz, M.; Sunshine, S. A. *Phys. Rev.* **1988**, *B37*, 7458.
(8) Matkin, D. I. In *Modern Oxide Materials*; Cockayne, B., Jones, D. W., Eds.; Academic Press: New York, 1972; p 235.
(9) Rao, C. N. R.; Rao, K. J. In *Solid State Compounds*, Cheetham A.-K., Day, P., Eds.; Clarendon Press: Oxford, U.K., 1992; p 281.
(10) Bierlein, J. D.; Arweiler, C. B. *Appl. Phys. Lett.* **1987**, *49*, 917.
(11) Centi, G.; Trifuro, F.; Ebner, J. R.; Franchetti, V. M. *Chem. Rev.* **1988**, *88*, 55.
(12) Grasselli, R. K. *Appl. Catal.* **1985**, *15*, 127.
(13) Gasior, M.; Gasior, I.; Grzybowska, B. *Appl. Catal.* **1984**, *10*, 87.
(14) Okuhara, T.; Misono, M. In *Encyclopedia of Inorganic Chemistry*; King, R. R., Ed.; John Wiley and Sons: New York, 1994; Vol. 6, p 2889.
(15) Niiyama, H.; Echigoya, E. *Bull. Chem. Soc. Jpn.* **1972**, *45*, 83.
(16) Yamaguchi, T. *Appl. Catal.* **1990**, *61*, 1.
(17) Clearfield, A. *Chem. Rev.* **1988**, *88*, 125.
(18) Newsam, J. M. In *Solid State Compounds*; Cheetham, A. K, Day, P., Eds.; Clarendon Press: Oxford, U.K., 1992; p 234.
(19) Ruthven, D. M. *Principles of Absorption and Absorption Processes*; Wiley-Interscience: New York, 1984.
(20) Szostak, R. *Molecules Sierves-Principles of Synthesis and Identification*; Van Nostrand Rheinhold: New York, 1988.
(21) Raleo, J. A. *Zeolite Chemistry and Catalysis*; ACS Monograph (7); American Chemical Society: Washington, DC, 1976.
(22) Murakami, Y.; Iijima, A.; Ward, J. W. *New Developments in Zeolite Science*; Elsevier: Amsterdam, 1986.
(23) Vaughan, D. E. W. *Properties and Applications of Zeolites*; Chem. Soc. Special Publ. No. 33; Townsend, R. P., Ed.; The Chemical Society: London, 1979; p 294. Cheetham, A. K. *Science* **1994**, *264*, 794.
(24) Venuto, P. B. *Microporous Mater*. **1994**, *2*, 297.
(25) (a) Smith, J. V. *Chem. Rev.* **1988**, *88*, 149−182. (b) Occelli, M. L.; Robson, H. C. *Zeolite Synthesis*; American Chemical Society: Washington, DC, 1989.
(26) Mann, S. *Nature* **1993**, *365*, 499.
(27) Kresge, C. T.; Leonowicz, M. E.; Roth, W. J.; Vartuli, J. C.; Beck, J. S. *Nature* **1992**, *359*, 710.
(28) Haushalter, R. C.; Mundi, L. A. *Chem. Mater.* **1992**, *4*, 31.
(29) Khan, M. I.; Meyer, L. M.; Haushalter, R. C.; Schweitzer, C. L.; Zubieta, J.; Dye, J. L. *Chem. Mater.* **1996**, *8*, 43.
(30) Zhang, Y.; DeBord, J. R. D.; O'Connor, C. J.; Haushalter, R. C.; Clearfield, G.; Zubieta, J. *Angew. Chem., Int. Ed. Engl.* **1996**, *35*, 989.
(31) DeBord, J. R. D.; Haushalter, R. C.; Meyer, L. M.; Rose, P. J.; Zapf, P.; Zubieta, J. *Inorg. Chem. Acta* **1997**, *256*, 165.
(32) Hagrman, D.; Sangregorio, C.; O'Connor, C. J.; Zubieta, J. *J. Chem. Soc., Dalton Trans.* **1999**, 3707.
(33) Hagrman, D.; Zapf, P. J.; Zubieta, J. *Chem. Commun.* **1998**, 1283.

10.1021/ic0002162 CCC: $19.00
Published on Web 10/21/2000

polymeric coordination complex cations;[36,37](c) solids exhibiting complex transition metal/organic components as peripheral moieties or bridging subunits of the oxide microstructure.[38−43] Representative examples of the latter class of inorganic oxides are provided by the vanadium oxides [{Zn(2,2′-bpy)}$_2$V$_6$O$_{17}$],[30] [Cu(2,2′-bpy)V$_2$O$_6$],[44] and [Cu$_3$(triazolate)$_2$V$_4$O$_{12}$].[45] Examples of molybdenum oxides include [Ni(2,2′-bpy)$_2$Mo$_4$O$_{13}$],[38] [Cu(2,2′-bpy)Mo$_2$O$_7$],[38] [Cu(2,2′-bpy)Mo$_3$O$_{10}$],[38] and the family of one-dimensional iron molybdates [FeCl(2,2′-bpy)MoO$_4$], [{Fe(2,2′-bpy)}$_2$Mo$_3$O$_{12}$], and [{Fe(2,2′-bpy)}$_2$Mo$_4$O$_{15}$].[42]

The structural chemistry of such solid-state coordination compounds reflects the ligand geometry and the choice of the secondary metal center, that is, the metal coordinated to the ligand in the cationic coordination complex component. The interplay of ligand geometry and secondary metal coordination preferences may be exploited in the modification of the oxide structure. For example, the molybdenum oxide family of materials of the type M(II,III)−ligand/Mo/O where the ligand is 2,2′-bpy adopt one- or two-dimensional structures with the ligand serving to passivate the oxide surface with respect to extension into layered or framework materials, respectively. This dramatic influence of the 2,2′-bpy ligand on the structures of such bimetallic oxides encouraged us to extend the study to the 2,2′:6′,2″-terpyridine ligand (terpy) which by virtue of its tridentate meridional coordination mode might be expected to impose considerable steric constraints on the oxide substructure. The geometric demands of the ligand exert a significant influence on the structures of the materials of the M(II)−ligand/Mo/O class of materials represented by [Cu(terpy)MoO$_4$]·3H$_2$O (**MOXI-40**), [Cu(terpy)Mo$_2$O$_7$] (**MOXI-41**), [Zn(terpy)Mo$_2$O$_7$] (**MOXI-42**), and [{Fe(terpy)}$_2$Mo$_3$O$_{12}$]·H$_2$O (**MOXI-43**·H$_2$O).

Experimental Section

Reagents were purchased from Aldrich Chemical Co. and used without further purification. All syntheses were carried out in 23 mL poly(tetrafluoroethylene)-lined stainless steel containers under autogenous pressure. The reactants were stirred briefly before heating. All distilled water used was distilled above 3.0 Ω in-house using a Barnstead model 525 Biopure Distilled Water Center.

Synthesis of [Cu(terpy)MoO$_4$]·3H$_2$O (MOXI-40). A solution of Na$_2$MoO$_4$·2H$_2$O (0.1609 g, 0.665 mmol), CuSO$_4$·5H$_2$O(0.0550 g, 0.220 mmol), 2,2′:6′,2″-terpyridine (0.0528 g, 0.227 mmol), and H$_2$O (8.0336 g, 446.3 mmol) was heated for 72 h at 160 °C. Large blue blocks of **MOXI-40** were separated by the Pasteur method from green plates of [Cu(terpy)Mo$_2$O$_7$](**MOXI-41**). The yields of **MOXI-40** and **MOXI-41** were ca. 30% and 12% based on Mo.

Synthesis of [Cu(terpy)Mo$_2$O$_7$] (MOXI-41). As noted above green plates of **MOXI-41** appeared as a byproduct of the synthesis of **MOXI-40**. Attempts to optimize the synthesis of **MOXI-41** proved only marginally successful. In the most effective synthesis, a solution of Na$_2$MoO$_4$·2H$_2$O (0.1081 g, 0.447 mmol), CuSO$_4$·5H$_2$O (0.0548 g, 0.220 mmol), 2,2′:6′,2″-terpyridine (0.0528 g, 0.216 mmol), and H$_2$O (8.0144 g, 445.2 mmol) was heated at 160 °C for 72 h. Green plates of **MOXI-41** in ca. 20% yield were separated from a mass of blue blocks of **MOXI-40.**

Synthesis of [Zn(terpy)Mo$_2$O$_7$] (MOXI-42). A solution of Na$_2$MoO$_4$·2H$_2$O (0.0520 g, 0.215 mmol), ZnCl$_2$ (0.0307 g, 0.225 mmol), 2,2′:6′,2″-terpyridine (0.0527 g, 0.227 mmol), and H$_2$O (8.0854 g, 449.2 mmol) was heated at 160 °C for 72 h. After cooling of the reaction for 3 h, **MOXI-42** was isolated as yellow plates in ca. 30% yield. The product was separated mechanically from a small amount of yellow rods of [ZnCl$_2$(terpy)].

Synthesis of [{Fe(terpy)}$_2$Mo$_3$O$_{12}$]·H$_2$O (MOXI-43·H$_2$O). A solution of Na$_2$MoO$_4$·2H$_2$O (0.0857 g, 0.354 mmol), FeCl$_2$·4H$_2$O (0.0722 g, 0.363 mmol), and H$_2$O (8.0130 g, 445.2 mmol) was heated at 160 °C for 78 h. Yellow shards of **MOXI-43** were isolated in ca. 10% yield.

Thermal Decomposition Studies. Thermogravimetric studies were performed on 8−15 mg samples under a 50 mL/min flow of air; the temperature was ramped from 20 to 600 °C at a rate of 5 °C/min. In all cases, a weight loss corresponding to the loss of ligand was observed at ca. 350−450 °C. The residues proved to be amorphous in XRD studies. Elemental analyses suggested that these residues are mixtures of oxides.

X-ray Crystallography. Structural measurements for compounds **MOXI-40, -41, -42,** and **-43** were performed on a Siemens SMART-CCD diffractometer using graphite-monochromated Mo Kα radiation (λ(Mo Kα) = 0.710 73 Å). The data for **MOXI-40**−**43** were collected at a temperature of 150 ± 1 K and were corrected for Lorentz and polarization effects. The structures of **MOXI-40, -41,** and **43** were solved by direct methods[46] while that of **MOXI-42** was solved by utilizing the Patterson method. All non-hydrogen atoms in **MOXI-40**−**43** were refined anisotropically. Neutral atom scattering coefficients and anomalous dispersion corrections were taken from ref 47. All calculations were performed using the SHELXTL[48] crystallographic software package except as described for **MOXI-42**, below.

Crystals of compound **MOXI-42** exhibited nonmerohedral twinning which required the use of a set of programs supplied with the Windows NT SHELXTL package by Bruker Analytical X-ray Systems, Inc. Using the program SAINT[49] with each of two contributing orientation matrixes and the frames of raw data collected by SMART,[50] two sets of integrated intensities were generated. Using the program TWHKL,[51] each reflection from the two sets was placed into one of three categories: (1) reflections from the two twin components with almost exact overlap; (2) reflections from the two twin components with partial overlap; (3) reflections from the two twin components which do not overlap. Two sets of indices (one from each component) were assigned to those reflections in the first category. One set of indices was assigned to those reflections in the third category. The reflections in the second category were discarded. TWHKL generated a file containing reflection indices and squared structure factors from the first and third categories. This file was then used as input to SHELXTL which did a least-squares refinement of the atomic parameters. This program also refined the volume fraction of one of the twin components. Finally, the program TWROT[27] determined the rotation axis for the twinning operation from the two orientation matrixes. It was determined that the orientation of

(34) LaDuca, R. L., Jr.; Rarig, R. S.; Zapf, P.; Zubieta, J. *Inorg. Chim. Acta* **1999**, *292*, 131.
(35) Hagrman, D.; Zubieta, J. *Chem. Commun.* **1998**, 2005.
(36) Hagrman, D.; Zubieta, C.; Haushalter, R. C.; Zubieta, J. *Angew. Chem., Int. Ed. Engl.* **1997**, *36*, 873.
(37) Hagrman, D.; Zubieta, J. *Chem. Commun.* **1998**, 2005.
(38) Zapf, P. J.; Warren, C. J.; Haushalter, R. C.; Zubieta, J. *Chem. Commun.* **1997**, 1543.
(39) Hagrman, D.; Haushalter, R. C.; Zubieta, J. *Chem. Mater.* **1998**, *10*, 361.
(40) Hagrman, D.; Warren, C. J.; Haushalter, R. C.; Seip, C.; O'Connor, C. J.; Rarig, R. S., Jr.; Johnson, K. M., III; LaDuca, R. L., Jr.; Zubieta, J. *Chem. Mater.* **1998**, *10*, 3294.
(41) Zapf, P. J.; Haushalter, R. C.; Zubieta, J. *Chem. Mater.* **1997**, *9*, 2019.
(42) Zapf, P. J.; Hammond, R. P.; Haushalter, R. C.; Zubieta, J. *Chem. Mater.* **1998**, *10*, 1366.
(43) Zapf, P. J.; LaDuca, R. C. Jr.; Rarig, R. S.; Johnson, K. M.; Zubieta, J. *Inorg. Chem.* **1998**, *37*, 3411.
(44) DeBord, J. R. D.; Zhang, Y.; Haushalter, R. C.; Zubieta, J.; O'Connor, C. J. *J. Solid State Chem.* **1996**, *122*, 251.
(45) Hagrman, P. J.; Bridges, C.; Greedan, J. E.; Zubieta, J. *J. Chem. Soc., Dalton Trans.* **1999**, 2901.
(46) SHELXTL PC Siemens Analytical X-ray Instruments, Inc., Madison, WI, 1993.
(47) *International Tables for Crystallography*; Kluwer Academic Publishers: Dordrecht, 1989; Vol. C, Tables 4.2.6.8 and 6.1.1.4.
(48) Sheldrick, G. M. *SHELXTL PC. Version 5.0*; Siemens Analytical Instruments Inc.: Madison, WI, 1994.
(49) *SAINT Data Reduction Software. Version 4.050;* Siemens Analytical Instruments Inc.: Madison, WI, 1996.
(50) *SMART. Data Collection Software. Version 4.050*; Siemens Analytical Instruments Inc.: Madison, WI, 1996.
(51) Sparks, R. A. *TWINDX, TWUTIL, TWHKL, TWROT. Nonmerohedral Twinning Software. Beta test version*; Bruker Analytical X-ray Systems, Inc.: Madison, WI, 1997.

Table 1. Summary of Crystallographic Data for the Structures of $[Cu(terpy)MoO_4]\cdot 3H_2O$ (MOXI-40), $[Cu(terpy)Mo_2O_7]$ (**MOXI-41**), $[Zn(terpy)Mo_2O_7]$ (**MOXI-42**), and $[\{Fe(terpy)\}_2Mo_3O_{12}]$ (**MOXI-43**)

	MOXI-40	**MOXI-41**	**MOXI-42**	**MOXI-43**
chem formula	$C_{15}H_{17}CuMoN_3O_7$	$C_{15}H_{11}CuMo_2N_3O_7$	$C_{15}H_{11}Mo_2N_3O_7Zn$	$C_{30}H_{24}Fe_2Mo_3N_6O_{13}$
a, Å	15.6145(3)	9.4860(2)	8.6984(7)	16.5820(8)
b, Å	12.4036(2)	9.8437(1)	10.3068(8)	11.0229(5)
c, Å	18.7990(1)	10.9604(3)	11.1165(8)	20.079(1)
α, deg	90.0	66.711(1)	91.655(1)	90.0
β, deg	97.084(1)	86.387(1)	110.740(1)	106.056(1)
γ, deg	90.0	68.479(1)	112.174(1)	90.0
V, Å^3	3613.12(9)	870.49(3)	847.8(1)	3526.9(3)
Z	8	2	2	4
fw	510.80	582.00	602.52	1076.07
space group	*C*2/*c*	P1	P1	$P2_1/n$
T, K	150	150	150	150
λ, Å	0.710 73	0.710 73	0.710 73	0.710 73
D_{calc}, g cm^{-3}	1.878	2.292	2.360	2.027
μ, mm^{-1}	1.915	2.680	2.908	1.914
R1[a]	0.0358	0.0674	0.0628	0.0649
WR2[b]	0.0806	0.1298	0.1375	0.1103

[a] $\Sigma||F_o| - |F_c||/|F_o|$. [b] $[\Sigma[w(F_o^2 - F_c^2)^2]/\Sigma[w(F_o^2)_2]]^{1/2}$.

Table 2. Selected Bond Lengths (Å) and Angles (deg) for $[Cu(terpy)MoO_4]\cdot 3H_2O$ (**MOXI-40**$\cdot 3H_2O$)[a]

Mo(1)−O(1)	1.745(2)	Cu(2)−N(2)	1.941(2)
Mo(1)−O(2)	1.756(2)	Cu(2)−N(3)	2.037(3)
Mo(1)−O(3)	1.789(2)	Cu(2)−N(1)	2.038(3)
Mo(1)−O(4)	1.794(2)	Cu(2)−O(4)	2.189(2)
Cu(2)−O(3)#1[a]	1.893(2)	O(3)−Cu(2)#1[a]	1.893(2)
O(1)−Mo(1)-O(2)	108.26(11)	O(3)#1−Cu(2)−N(1)	98.40(10)
O(1)−Mo(1)−O(3)	109.59(11)	N(2)−Cu(2)−N(1)	79.87(11)
O(2)−Mo(1)−O(3)	109.06(11)	N(3)−Cu(2)−N(1)	159.32(10)
O(1)−Mo(1)−O(4)	110.27(10)	O(3)#1−Cu(2)−O(4)	96.34(9)
O(2)−Mo(1)−O(4)	108.06(10)	N(2)−Cu(2)−O(4)	101.90(9)
O(3)−Mo(1)−O(4)	111.53(10)	N(3)−Cu(2)−O(4)	97.30(9)
O(3)#1−Cu(2)−N(2)[a]	161.74(11)	N(1)−Cu(2)−O(4)	92.86(9)
O(3)#1−Cu(2)−N(3)[a]	98.32(10)	Mo(1)−O(3)−Cu(2)#1[a]	169.52(15)
N(2)−Cu(2)−N(3)	80.44(11)	Mo(1)O(4)−Cu(2)	125.07(11)

[a] Symmetry transformations used to generate equivalent atoms: #1, $-x$, y, $-z + 1/2$.

the second twin component is related to the first by a rotation of 180° about the normal to the 001 face of the crystal. After the use of Sparks' Non-merohedral Twinning Software, refinement of the solution for **MOXI-42** was unexceptional.

Crystallographic data for **MOXI-40**−**43** are listed in Table 1. Atomic positional parameters and isotropic temperature factors for MOXI-40−43 are given in the Supporting Information. Selected bond lengths and angles for **MOXI-40**−**43** are listed in Tables 2−5.

Results and Discussion

The synthetic methodology derives from our general approach of employing organic components to modify the crystallization of metal oxides in a hydrothermal medium. Working in the hydrothermal domain allows us to overcome problems associated with the differential solubilities of the reactants. Furthermore, the reduced viscosity of water under these conditions enhances the solvent extraction of solids and the rate of crystallization from solution.

The hydrothermal reaction of $Na_2MoO_4\cdot 2H_2O$, $CuSO_4\cdot 5H_2O$, 2,2′:6′,2″-terpyridine (terpy), and H_2O in the mole ratio 3.0:1.1:1.0:2013 at 160 °C for 72 h produced a mixture of large blue blocks of $[Cu(terpy)MoO_4]\cdot 3H_2O$ (**MOXI-40**) and green plates of $[Cu(terpy)Mo_2O_7]$(**MOXI-41**). Attempts to optimize the synthesis and to prepare monophasic materials proved generally unsuccessful. The yield of **MOXI-41** relative to **MOXI-40** was improved by altering the stoichiometry of the reaction to the mole ratio 2.0:1.0:1.0:1994 for $Na_2MoO_4\cdot 2H_2O$, $CuSO_4\cdot 5H_2O$, terpy, and H_2O, respectively.

As often observed in hydrothermal syntheses, there is no apparent correlation between the composition of the product and reaction stoichiometries employed. However, it is clear that the identity of the product obtained in hydrothermal reactions is critically dependent on the specific reaction conditions employed, as evidenced by the lack of success in synthesizing MOXI-40 and **MOXI-41** using MoO_3 and/or $CuCl_2\cdot 2H_2O$ as the starting materials.

To assess the influence of the coordination preferences of other metal centers on the product structures, the reactions of Zn(II) and Fe(II) with $NaMoO_4\cdot 2H_2O$ and terpy were investigated. The reaction of $Na_2MoO_4\cdot 2H_2O$, $ZnCl_2$, terpy, and H_2O in the mole ratio 1.0:1.05:1.05:2090 at 160 °C for 72 h yielded $[Zn(terpy)Mo_2O_7]$ (MOXI-42) as yellow plates. Similarly, the reaction of $Na_2MoO_4\cdot 2H_2O$, $FeCl_2\cdot 4H_2O$, terpy, and H_2O in the mole ratio 2:0:1.0:2.1:2514 at 160 °C for 78 h produced $[\{Fe(terpy)\}_2Mo_3O_{12}]\cdot H_2O$ (**MOXI-43**$\cdot H_2O$) as yellow shards in low yield.

The structure of $[Cu(terpy)MoO_4]$ (**MOXI-40**) consists of a bimetallic tetranuclear cluster, shown in Figure 1. The cluster is constructed from corner-sharing $\{MoO_4\}^{2-}$ tetrahedra and $\{CuN_3O_2\}$ square pyramids, with a cyclic $\{Cu_2Mo_2O_4\}$ core. The basal plane of the Cu square pyramid is defined by the three nitrogen donors of the terpy ligand and one bridging oxo group, while the apical position is occupied by the second bridging oxo group. This coordination geometry is reflected in Cu−O bond distances of 1.893(2) and 2.189(2) Å for the basal and apical positions, respectively. The steric constraints on the

Table 3. Selected Bond Lengths (Å) and Angles (deg) for [Cu(terpy)Mo_2O_7] (**MOXI-41**)[a]

Cu(1)−O(1)	1.914(7)	Mo(1)−O(4)	1.883(8)
Cu(1)−N(2)	1.940(8)	Mo(1)−O(5)#2[a]	2.324(8)
Cu(1)−N(3)	2.015(8)	Mo(2)−O(7)	1.709(9)
Cu(1)−N(1)	2.024(9)	Mo(2)−O(6)	1.715(9)
Cu(1)−O(3)#1[a]	2.179(7)	Mo(2)−O(5)	1.921(8)
Mo(1)−O(2)	1.719(9)	Mo(2)−O(4)	1.926(8)
Mo(1)−O(3)	1.746(7)	Mo(2)−O(5)#2	2.066(8)
Mo(1)−O(1)	1.781(7)		
O(1)−Cu(1)−N(2)	156.7(3)	O(7)−Mo(2)−O(5)	105.2(4)
O(1)−Cu(1)−N(3)	98.0(3)	O(6)−Mo(2)−O(5)	99.1(4)
N(2)−Cu(1)−N(3)	80.5(3)	O(7)−Mo(2)−O(4)	99.8(4)
O(1)−Cu(1)−N(1)	97.7(3)	O(6)−Mo(2)−O(4)	98.2(4)
N(2)−Cu(1)−N(1)	80.2(3)	O(5)−Mo(2)−O(4)	143.4(4)
N(3)−Cu(1)−N(1)	160.0(3)	O(7)−Mo(2)−O(5)#2[a]	114.8(4)
O(1)−Cu(1)−O(3)#1[a]	99.9(3)	O(6)−Mo(2)−O(5)#2[a]	137.6(4)
N(2)−Cu(1)−O(3)#1[a]	103.3(3)	O(5)−Mo(2)−O(5)#2[a]	73.3(4)
N(3)−Cu(1)−O(3)#1[a]	98.9(3)	O(4)−Mo(2)−O(5)#2[a]	72.2(3)
N(1)−Cu(1)−O(3)#1[a]	90.4(3)	O(7)−Mo(2)−Mo(2)#2[a]	115.3(3)
O(2)−Mo(1)−O(3)	105.7(4)	O(6)−Mo(2)−Mo(2)#2[a]	124.9(3)
O(2)−Mo(1)−O(1)	111.9(4)	O(5)−Mo(2)−Mo(2)#2[a]	38.2(2)
O(3)−Mo(1)−O(1)	105.7(3)	O(4)−Mo(2)−Mo(2)#2[a]	106.6(3)
O(2)−Mo(1)−O(4)	114.1(4)	O(5)#2−Mo(2)−Mo(2)#2[a]	35.1(2)
O(3)−Mo(1)−O(4)	96.6(3)	Mo(1)−O(1)−Cu(1)	147.8(4)
O(1)−Mo(1)−O(4)	120.1(4)	Mo(1)−O(3)−Cu(1)#1[a]	146.0(4)
O(2)−Mo(1)−O(5)[a]	83.0(4)	Mo(1)−O(4)−Mo(2)	121.0(5)
O(3)−Mo(1)−O(5)#2[a]	163.7(3)	Mo(2)−O(5)−Mo(2)#2[a]	106.7(4)
O(1)−Mo(1)−O(5)#2[a]	83.0(3)	Mo(2)−O(5)−Mo(1)#2[a]	148.0(5)
O(4)−Mo(1)−O(5)#2[a]	67.2(3)	Mo(2)#2−O(5)Mo(1)#2[a]	97.9(3)
O(7)−Mo(2)−O(6)	107.5(5)		

[a] Symmetry transformations used to generate equivalent atoms: #1, $-x + 2$, $-y + 1$, $-z$; #2, $-x + 2$, $-y$, $-z + 1$.

Table 4. Selected Bond Lengths (Å) and Angles (deg) for [Zn(terpy)Mo_2O_7] (**MOXI-42**)[a]

Mo(1)−O(1)	1.711(4)	Mo(2)−O(6)#2	1.994(4)
Mo(1)−O(2)	1.720(5)	Mo(2)−O(6)	2.019(5)
Mo(1)−O(5)	1.858(4)	Zn(1)−O(5)	1.961(4)
Mo(1)−O(3)	1.892(4)	Zn(1)−O(6)	1.993(4)
Mo(1)−O(5)#1	2.299(5)	Zn(1)−N(2)	2.064(6)
Mo(2)−O(8)	1.702(4)	Zn(1)−N(3)	2.162(5)
Mo(2)−O(7)	1.715(5)	Zn(1)−N(1)	2.187(5)
Mo(2)−O(3)#1	1.935(4)		
O(1)−Mo(1)−O(2)	104.0(2)	O(6)#2−Mo(2)−O(6)	72.5(2)
O(1)−Mo(1)−O(5)	113.4(2)	O(5)−Zn(1)−O(6)	114.51(19)
O(2)−Mo(1)−O(5)	99.7(2)	O(5)−Zn(1)−N(2)	133.23(19)
O(1)−Mo(1)−O(3)	113.3(2)	O(6)−Zn(1)−N(2)	112.25(19)
O(2)−Mo(1)−O(3)	99.0(2)	O(5)−Zn(1)−N(3)	97.73(19)
O(5)−Mo(1)−O(3)	122.96(19)	O(6)−Zn(1)−N(3)	96.01(19)
O(1)−Mo(1)−O(5)#1	88.48(19)	N(2)−Zn(1)−N(3)	76.2(2)
O(2)−Mo(1)−O(5)#1	167.30(19)	O(5)−Zn(1)−N(1)	98.86(19)
O(5)−Mo(1)−O(5)#1	72.6(2)	O(6)−Zn(1)−N(1)	97.86(19)
O(3)−Mo(1)−O(5)#1	77.72(18)	N(2)−Zn(1)−N(1)	75.6(2)
O(8)−Mo(2)−O(7)	108.9(2)	N(3)−Zn(1)−N(1)	151.6(2)
O(8)−Mo(2)−O(3)#1	98.3(2)	Mo(1)−O(3)−Mo(2)#1	139.3(3)
O(7)Mo(2)−O(3)#1	97.9(2)	Mo(1)−O(5)−Zn(1)	132.1(2)
O(8)−Mo(2)−O(6)#2	98.43(19)	Mo(1)−O(5)−Mo(1)#1	107.4(2)
O(7)−Mo(2)−O(6)#2	95.6(2)	Zn(1)−O(5)−Mo(1)#1	117.5(2)
O(3)#1−Mo(2)−O(6)#2	153.8(2)	Zn(1)−O(6)−Mo(2)#2	125.0(2)
O(8)−Mo(2)−O(6)	121.6(2)	Zn(1)−O(6)−Mo(2)	126.1(2)
O(7)−Mo(2)−O(6)	129.2(2)	Mo(2)#2−O(6)−Mo(2)	107.54(19)
O(3)#1−Mo(2)−O(6)	81.6(2)		

[a] Symmetry transformations used to generate equivalent atoms: #1, −x, y + 1, −z; #2, −x, −y, −z.

terpy ligand concomitant to forming two five-membered chelate rings with the metal are manifested in the Cu−N distances of 1.941(2) Å to the central pyridyl nitrogen of the ligand and 2.038(3) Å (average) to the two outer pyridyl nitrogen donors.

The structure of MOXI-40 is reminiscent of that of [{Ni(2,2′-bpy)$_2$}$_2$$Mo_4O_{14}$], shown in Figure 2. The molecular cluster of this latter compound is constructed from corner-sharing {MoO_4} tetrahedra and {NiN_4O_2} octahedra, with a cyclic {$Ni_2Mo_4O_6$} core. The structure may be described as two {Mo_2O_7}$^{2-}$ dimers linked by two {Ni(bpy)$_2$}$^{2+}$ moieties. To date, we have been unsuccessful in the syntheses of the anologous Ni/terpy cluster [{Ni(terpy)}$_2$$Mo_4O_{14}$] or of the analogous Cu/bpy complex [{Cu(bpy)$_2$}$_2$$Mo_4O_{14}$].

The material [Cu(terpy)Mo_2O_7] (MOXI-41) was found to cocrystallize with **MOXI-40**. As shown in Figure 3a, the structure of MOXI-41 consists of a one-dimensional chain, constructed from {Mo_4O_{14}}$^{4-}$ clusters linked by {Cu(terpy)}$^{2+}$ moieties. As shown in Figure 3b, the {Mo_4O_{14}}$^{4-}$ cluster

Table 5. Selected Bond Lengths (Å) and Angles (deg) for [{Fe(terpy)}$_2$Mo$_3$O$_{12}$·H$_2$O] (**MOXI-43**·H$_2$O)[a]

Mo(1)−O(2)	1.723(5)	Fe(1)−O(5)	1.923(5)
Mo(1)−O(3)	1.735(5)	Fe(1)−O(10)$^{\#1}$	1.942(5)
Mo(1)−O(1)	1.809(5)	Fe(1)−O(1)	1.971(5)
Mo(1)−O(4)	1.820(5)	Fe(1)−N(2)	2.125(6)
Mo(2)−O(7)	1.702(5)	Fe(1)−N(1)	2.140(6)
Mo(2)−O(6)	1.733(5)	Fe(1)−N(3)	2.162(6)
Mo(2)−O(8)	1.809(5)	Fe(2)−O(4)	1.915(5)
Mo(2)−O(5)	1.825(5)	Fe(2)−O(9)	1.953(5)
Mo(3)−O(11)	1.710(5)	Fe(2)−O(8)	1.955(5)
Mo(3)−O(12)	1.738(5)	Fe(2)−N(5)	2.110(6)
Mo(3)−O(9)	1.812(5)	Fe(2)−N(6)	2.145(6)
Mo(3)−O(10)	1.812(5)	Fe(2)−N(4)	2.162(6)
O(2)−Mo(1)−O(3)	107.7(3)	N(2)−Fe(1)−N(1)	74.2(2)
O(2)−Mo(1)−O(1)	111.1(2)	O(5)−Fe(1)−N(3)	113.3(2)
O(3)−Mo(1)−O(1)	107.1(2)	O(10)$^{\#1}$−Fe(1)−N(3)	84.9(2)
O(2)−Mo(1)−O(4)	110.8(2)	O(1)−Fe(1)−N(3)	87.7(2)
O(3)−Mo(1)−O(4)	106.3(3)	N(2)−Fe(1)−N(3)	74.0(2)
O(1)−Mo(1)−O(4)	113.7(2)	N(1)−Fe(1)−N(3)	148.2(2)
O(7)−Mo(2)−O(6)	108.4(3)	O(4)−Fe(2)−O(9)	90.6(2)
O(7)−Mo(2)−O(8)	108.4(2)	O(4)−Fe(2)−O(8)	89.2(2)
O(6)−Mo(2)−O(8)	109.8(2)	O(9)−Fe(2)−O(8)	179.8(2)
O(7)−Mo(2)−O(5)	110.9(3)	O(4)−Fe(2)−N(5)	172.8(2)
O(6)−Mo(2)−O(5)	110.5(2)	O(9)−Fe(2)−N(5)	85.9(2)
O(8)−Mo(2)−O(5)	108.8(2)	O(8)−Fe(2)−N(5)	94.2(2)
O(11)−Mo(3)−O(12)	109.5(2)	O(4)−Fe(2)−N(6)	99.3(2)
O(11)−Mo(3)−O(9)	109.4(2)	O(9)−Fe(2)−N(6)	89.1(2)
O(12)−Mo(3)−O(9)	108.9(2)	O(8)−Fe(2)−N(6)	90.9(2)
O(11)−Mo(3)−O(10)	110.0(2)	N(5)−Fe(2)−N(6)	74.3(2)
O(12)−Mo(3)−O(10)	113.8(3)	O(4)−Fe(2)−N(4)	111.1(2)
O(9)−Mo(3)−O(10)	105.1(2)	O(9)−Fe(2)−N(4)	90.8(2)
O(5)−Fe(1)−O(10)$^{\#1}$	89.9(2)	O(8)−Fe(2)−N(4)	89.2(2)
O(5)−Fe(1)−O(1)	91.0(2)	N(5)−Fe(2)−N(4)	75.3(2)
O(10)$^{\#1}$−Fe(1)−O(1)	172.3(2)	N(6)−Fe(2)−N(4)	149.6(2)
O(5)−Fe(1)−N(2)	172.2(2)	Mo(1)−O(1)−Fe(1)	141.7(3)
O(10)$^{\#1}$−Fe(1)−N(2)	88.2(2)	Mo(1)−O(4)−Fe(2)	129.5(3)
O(1)−Fe(1)−N(2)	91.9(2)	Mo(2)−O(5)−Fe(1)	135.7(3)
O(5)−Fe(1)−N(1)	98.4(2)	Mo(2)−O(8)−Fe(2)	147.1(3)
O(10)$^{\#1}$−Fe(1)−N(1)	93.7(2)	Mo(3)−O(9)−Fe(2)	139.3(3)
O(1)−Fe(1)−N(1)	93.7(2)	Mo(3)O(10)−Fe(1)$^{\#2}$	129.0(3)

[a] Symmetry transformations used to generate equivalent atoms: #1, x −1/2, −y + 3/2, z − 1/2; #2, x + 1/2, −y + 3/2, z + 1/2.

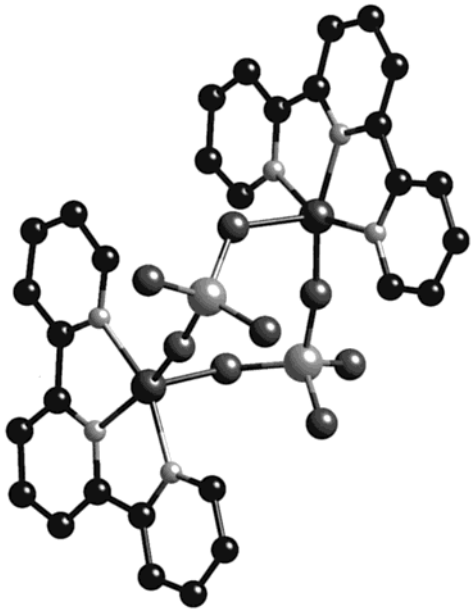

Figure 1. View of the structure of the tetranuclear cluster of [Cu(terpy)MoO$_4$] (**MOXI-40**).

consists of four edge- and corner-sharing {MoO$_5$} distorted square pyramids. The Cu(II) center exhibits a {CuN$_3$O$_2$} square

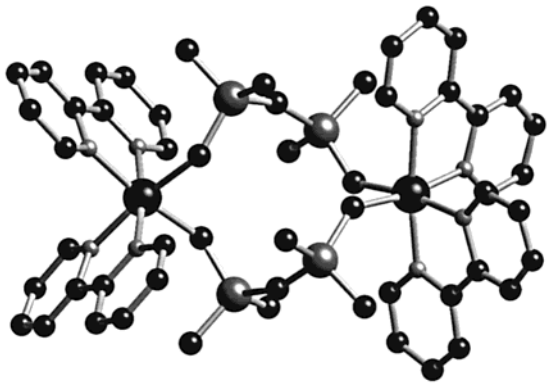

Figure 2. Structure of [{Ni(2,2′-bpy)$_2$}$_2$Mo$_4$O$_{14}$].

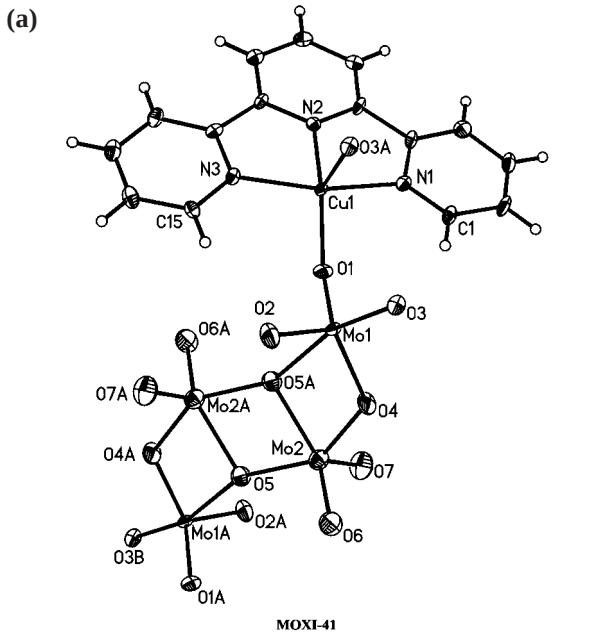

Figure 3. (a) Portion of the structure of [Cu(terpy)Mo$_2$O$_7$], showing the atom-labeling scheme and 50% thermal ellipsoids. (b) View of the one-dimensional chain structure of [Cu(terpy)Mo$_2$O$_7$] (MOXI-41). (c) {Mo$_4$O$_{14}$}$^{4-}$ cluster imbedded in the chain of **MOXI-41**.

pyramidal geometry similar to that of **MOXI-40**. The cyclic (Cu$_2$Mo$_2$O$_4$} motif of **MOXI-40** is also evident as a substructure

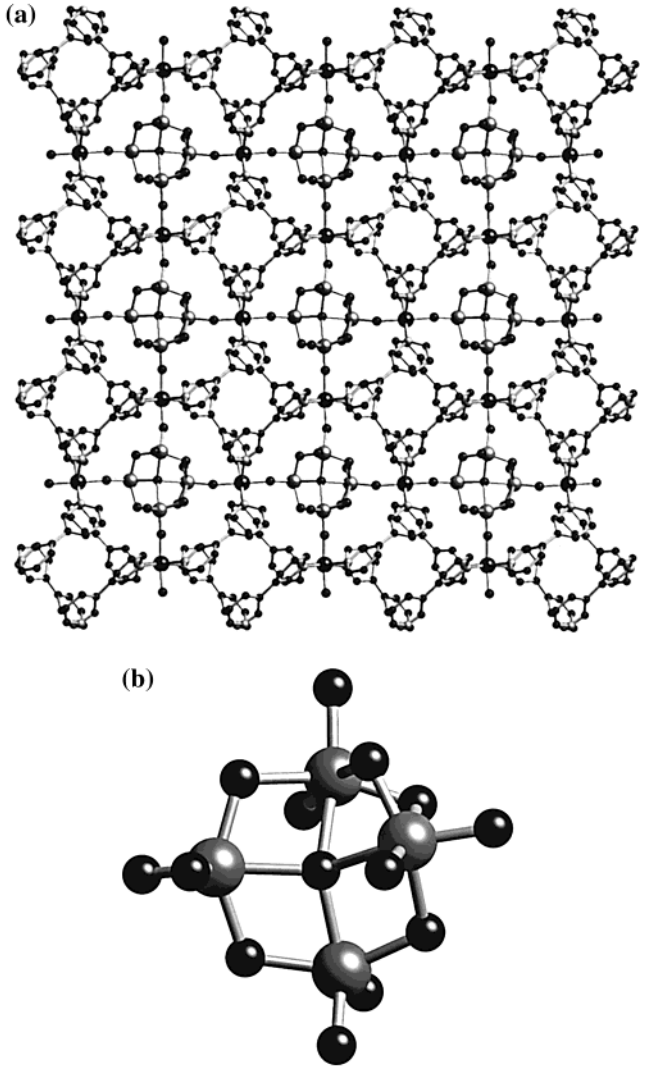

Figure 4. (a) View of the network structure of $[\{Ni(3,3'\text{-bpy})_2\}_2Mo_4O_{14}]$. (b) $\{Mo_4O_{14}\}^{4-}$ cluster imbedded in the chain.

of **MOXI-41**, whose structure may alternatively be described as $[\{Cu(terpy)\}_2\{MoO_4\}_2]$ clusters as in **MOXI-40**, linked through binuclear $\{Mo_2O_6\}$ subunits.

The $\{Mo_4O_{14}\}^{4-}$ cluster imbedded in the chain of **MOXI-41** is unusual in several respects. There is no precedent in the polyoxomolybdate chemistry for an isolated tetranuclear cluster. However, an imbedded tetramolybdate core has been reported in another example of a secondary metal−ligand−molybdate composite material $[\{Ni(3,3'\text{-bpy})_2\}_2Mo_4O_{14}]$,[52] illustrated in Figure 4a. In contrast to the extended structure of the $\{Mo_4O_{14}\}^{4-}$ cluster of **MOXI-41**, this latter cluster exhibits a tetrahedral arrangement of Mo(VI) centers around a central oxo-group, as shown in Figure 4b. Furthermore, the exclusively five-coordinate geometry is unanticipated for a molybdate core.

The profound influences of the coordination modes of the secondary metal site are revealed in the structure of [Zn(terpy)-Mo_2O_7] (**MOXI-42**). While **MOXI-41** and **MOXI-42** exhibit the identical stoichiometry, $[M(terpy)Mo_2O_7]$, the structures are quite distinct, as shown in Figure 5. The one-dimensional chain of **MOXI-42** consists of an undulating ribbon of edge- and corner-sharing $\{MoO_5\}$ square pyramids, decorated by peripheral $\{ZnN_3O_2\}$ square pyramids. The molybdate chain may be described in terms of binuclear $\{Mo_2O_8\}$ subunits of edge-sharing square pyramids, linked through corner-sharing of oxo groups in an anti disposition. The Zn(II) site links to the bridging oxo groups of two adjacent binuclear molybdate subunits to form a cyclic $\{ZnMo_2O_3\}$ moiety.

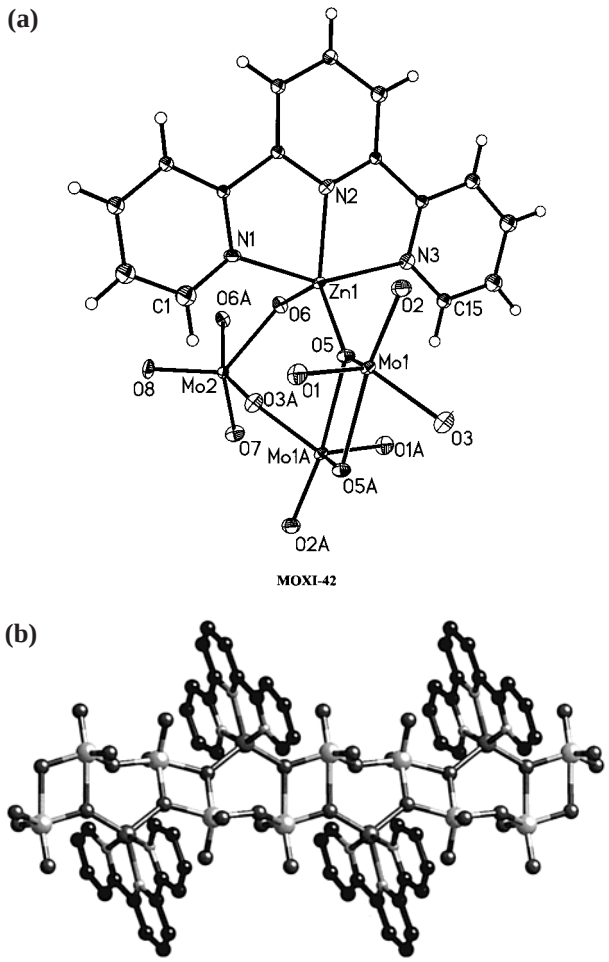

Figure 5. (a) Portion of the structure of $[Zn(terpy)Mo_2O_7]$, showing the atom-labeling scheme and 50% thermal ellipsoids. (b) One-dimensional structure of $[Zn(terpy)Mo_2O_7]$ (**MOXI-42**).

While the $\{ZnN_3O_2\}$ coordination geometry of **MOXI-42** is grossly similar to the $\{CuN_3O_2\}$ sites of **MOXI-40** and **MOXI-41**, the different geometric characteristics of the two metals are evident in the metrical parameters. The structural Jahn−Teller effect is commonly observed in Cu(II) complexes which tend to exhibit axially distorted "4 + 1" or "4 + 2" coordination geometries. The "4 + 1" geometry of the Cu(II) sites of **MOXI-40** and **MOXI-41** is manifested in the significantly longer Cu−O (apical) bond distances. In constrast, the Zn−O distances in **MOXI-42** are 1.961(4) and 1.993(4) Å for the basal and apical oxygens, respectively.

The structure of $[\{Fe(terpy)\}_2Mo_3O_{12}]\cdot H_2O$ (**MOXI-43**·H_2O) illustrates the preference of Fe(III) for octahedral coordination and the concomitant modification of the oxide substructure. As shown in Figure 6, the structure of **MOXI-43** is a one-dimensional chain of corner-sharing $\{MoO_4\}$ tetrahedra and $\{FeN_3O_3\}$ octahedra. The structure exhibits the $[\{M(terpy)\}_2$-$\{MoO_4\}_2]$ motif with the cyclic $\{M_2Mo_2O_4\}$ core common to **MOXI-40** and **MOXI-41**. Consequently, the structure may be described as $[\{Fe(terpy)\}_2(MoO_4)_2]^{2+}$ clusters bridged by $\{MoO_4\}^{2-}$ subunits.

(52) LaDuca, R. L., Jr.; Desciak, M.; Laskoski, M.; Rarig, R. S., Jr.; Zubieta, J. Unpublished results.

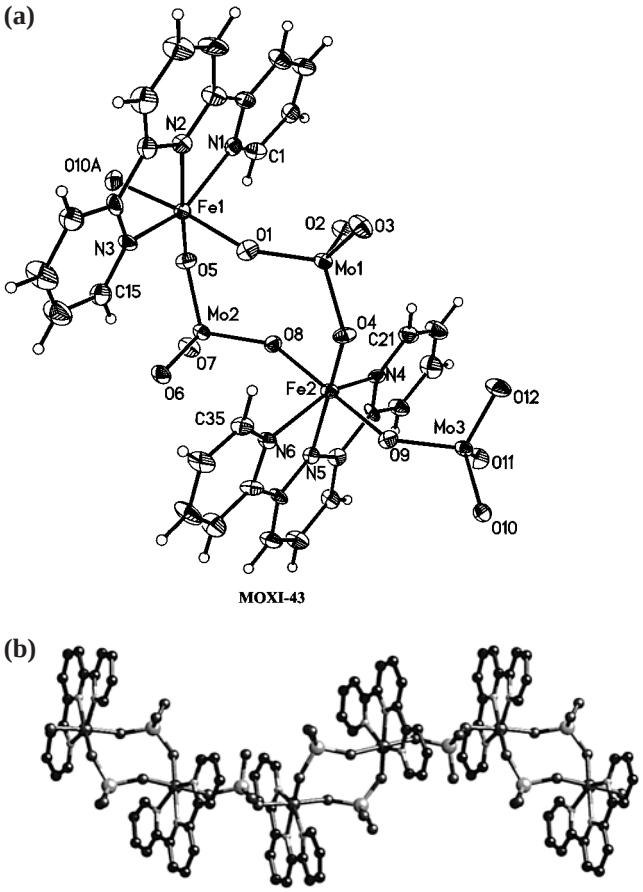

Figure 6. (a) Asymmetric unit of $[\{Fe(terpy)\}_2Mo_3O_{12}]$, showing the atom-labeling scheme and 50% thermal ellipsoids. (b) Structure of $[\{Fe(terpy)\}_2Mo_3O_{12}]\cdot H_2O$ (**MOXI-43**).

The persistence of the $[\{M(ligand)\}_2\{MoO_4\}_2]$ building block is apparent in these bimetallic oxide phases. This structural motif is also observed in the one-dimensional structures $[FeCl(2,2'\text{-bpy})MoO_4]$, $[\{Fe(2,2'\text{-bpy})\}_2Mo_3O_{12}]$, and $[\{Fe(2,2'\text{-bpy})\}_2Mo_4O_{15}]$. However, the versatility of molybdenum oxide coordination geometry and aggregation modes renders prediction of structure of such phases problematic. Thus, in the structures of **MOXI-40**−**43**, three distinct molybdate subunits are observed: isolated $\{MoO_4\}^{2-}$ tetrahedra; $\{Mo_4O_{14}\}^{4-}$ clusters; $\{Mo_2O_7\}_n^{2n-}$ chains. The observed structures are metastable phases which reflect the crystallization conditions as well as the coordination preferences of the metal sites and the ligand geometric constraints.

The high incidence of one-dimensional phases in the M(II,III)/polypyridyl/Mo/O system suggests that such bidentate and tridentate ligand types serve a passivating role by occupying coordination sites on the secondary metal site and providing steric constraints, thus preventing spatial extension of the oxide in two- or three-dimensions. In this sense, some degree of synthetic control has been introduced.

Conclusions

The isolation and characterization of compounds **MOXI-40**−**43** reinforce the observation that small amounts of organic material may profoundly influence the structures of metal oxide phases. It is evident that the combination of hydrothermal techniques and incorporation of organic components affords a powerful method for the modification of metal oxide structures and for the isolation of new metal oxide compositions. While it is premature to refer to such chemistry as "crystal engineering",[53] judicious choice of organic constituents allows for passivation of metal oxide coordination spheres leading to low-dimensional materials, variable tethering of oxide sites, sculpting of cavities, and preparation of unexpected mixed-metal/oxide/ligand composites. While predictability is yet lacking, structural and compositional diversity are not.

Acknowledgment. The work at Syracuse University was supported by NSF Grant CHE9617232.

Supporting Information Available: Tables of experimental details, atomic coordinates and temperature factors, anisotropic temperature factors, bond lengths and angles, and calculated hydrogen atom positions for compounds MOXI-40−43. This material is available free of charge via the Internet at http://pubs.acs.org.

IC0002162

(53) "Crystal engineering" is here used in the broadest sense of modification of the extended structure of a material. The organic components in the hybrid materials of this study allow isolation of bimetallic oxide chains which are otherwise inaccessible in the M(II)/Mo/O solid-state chemistry.